



1 Evaluating Yangtze River Delta Urban Agglomeration 2 flood risk using hybrid method of AutoML and AHP

3 Yu Gao^{1,2}, Haipeng Lu^{1,2}, Yaru Zhang^{1,2}, Hengxu Jin^{1,2}, Shuai Wu³, Yixuan Gao^{1,2},
4 Shuliang Zhang^{1,2*}

5 1 Key Laboratory of VGE of Ministry of Education, Nanjing Normal University, Nanjing 210023, China

6 2 Jiangsu Center for Collaborative Innovation in Geographical Information Resource Development and
7 Application, Nanjing 210023, China

8 3 Lianyungang Real Estate Registry, Lianyungang 222006, China

9 Correspondence to: Shuliang Zhang (zhangshuliang@njnu.edu.cn)

10 **Abstract.** With rapid urbanization, the scientific assessment of disaster risk caused by flooding events
11 has become an essential task for disaster prevention and mitigation. However, adaptively selecting
12 optimal machine learning (ML) models for flood risk assessment and further conducting spatial and
13 temporal analyses of flood risk characteristics in urban agglomerations remains challenging. This study,
14 establishes a “H–E–V–R” risk assessment index system that integrates hazard, exposure, vulnerability,
15 and resilience based on the factors influencing flood risk in the Yangtze River Delta Urban
16 Agglomeration (YRDUA). Utilizing Automated Machine Learning (AutoML) and the Analytic
17 Hierarchy Process (AHP), a comprehensive flood risk assessment model is constructed. Results indicate
18 that, among those of different assessment models, the accuracy, precision, F1-score, and kappa
19 coefficient of the CatBoost model for flooded point identification are the highest. Among the flood hazard
20 factors, elevation ranks highest in importance, with a contribution rate of up to 68.55%. The spatial
21 distribution of flood risk in the study area from 1990 to 2020 is heterogeneous, with an overall increasing
22 risk trend. This study is of great significance for advancing disaster prevention, mitigation, and
23 sustainable development in the YRDUA.

24 1 Introduction

25 Under global climate change and accelerated urbanization, China has been experiencing pervasive
26 flooding ever more frequently (Tang et al., 2024). Floods threaten people's lives, hinder social
27 development and cause huge economic losses in China (Anon, 2021; Echendu, 2020; Milanesi et al.,
28 2015). Flood formation has been exacerbated by climate change and urbanization, leading to increased
29 frequency, extent, and intensity of urban flooding, and impacting urban flood risk. (Mahmoud and Gan,
30 2018; Khadka et al., 2023; Scott et al., 2023; Seemuangngam and Lin, 2024). Modern human society is
31 faced with the possibility of serious flood hazards and associated challenges, and in addition to post-
32 disaster emergency management, the scientific assessment of disaster risks arising from flood events has
33 gradually become a crucial aspect in preventing and mitigating disasters.



34 Currently, most research in the field of flooding focuses on the flood risks of individual cities. (Wang et
35 al., 2021, 2023c; Guan et al., 2024). However, in recent years, the frequency and intensity of urban
36 flooding in China have increased dramatically, and individual cities are no longer able to independently
37 mitigate the risks arising from floods. Studies indicate that China's flood risk management needs to be
38 transformed from the scale of isolated individual cities to the scale of urban agglomerations, conducted
39 in a regionally coordinated manner (Morales-Torres et al., 2016; Wang et al., 2023b). City clusters,
40 constituting the spatial organizational structure of cities that have reached an advanced stage of
41 development, have become key areas for regional disaster management and sustainable development.
42 Due to the unique geographical location and climate conditions of the YRDUA, as well as the impact of
43 urbanization over the past 30 years, the frequency and intensity of flood disasters have been increasing,
44 posing a serious threat to the sustainable development of cities. Therefore, implementing relevant
45 emergency management strategies for flood risks is urgently needed. Furthermore, the region comprises
46 multiple cities, among which distinct resource interactions, such as population mobility and risk transfer,
47 exist (Lu et al., 2022). Thus, it is essential to assess both the overall flood risk characteristics and changes
48 in the urban agglomeration, as well as the spatial correlations of flood risks between cities, explore the
49 mutual influences and interaction mechanisms among regional disaster risks, and provide a scientific
50 basis for sustainable development within the urban agglomeration(Xu et al., 2024).

51 Statistical analyses of historical disaster statistics(Lang et al., 2004), indicator systems methods(Wang et
52 al., 2018), scenario simulations methods(Yang et al., 2018), and data-driven methods(Abu-Salih et al.,
53 2023), are the primary flood risk assessment method currently. With the development of artificial
54 intelligence technology, data-driven methods, such as machine learning, deep learning, and artificial
55 neural networks, have emerged, providing new opportunities for improving traditional flood risk
56 assessment methods (Liu Jiafu and Zhang Bai, 2015). As ML algorithms continue to develop and
57 improve, integrated methods address the limitations of general ML models have emerged (Kazienko et
58 al., 2015). Various integrated ML methods have been utilized in hydrology, with the Boost algorithm
59 being extensively applied for flood prediction and assessment (Shafizadeh-Moghadam et al., 2018;
60 Mirzaei et al., 2021; Yan et al., 2024). However, these integrated models lack preprocessing and feature
61 selection capabilities, and their application effects vary considerably across different regions. To fully
62 mine data and discover more effective features, experts have proposed other solutions, namely hybrid



63 models such as ANFIS, LSTM-ALO, and LSSVM-GSA (Nayak et al., 2004; Yuan et al., 2018; Adnan
64 et al., 2017). These methods have achieved good performances for given hydrological time series,
65 focusing more on data preprocessing and feature selection. Although research on data-driven urban flood
66 risk assessment methods has increased, certain limitations remain. For example, the physical importance
67 of urban hydrological processes is often ignored in the model assessment process, interpretation of the
68 assessment results is weak, and quantifying the boundaries and scales is challenging (Abu-Salih et al.,
69 2023; Guo et al., 2022).

70 Furthermore, attempting to combine the data processing and feature selection capabilities of hybrid
71 models with those of integrated models remains challenging (Li et al., 2017). Existing algorithms cannot
72 perform well for all learning problems; thus, each ML component, such as feature engineering, model
73 selection, and algorithm selection, must be carefully configured (Li et al., 2017; Raschka, 2020). Hence,
74 ML applications require the participation of many experts, leading to disproportionate costs for ML
75 development and improvement (Wagenaar et al., 2020; Sarro et al., 2022; Rashidi Shikhteymour et al.,
76 2023). Additionally, ML is not fully automated, and its application effect improves empirically (Jordan
77 and Mitchell, 2015; Nagarajah and Poravi, 2019). AutoML is an innovative ML framework designed for
78 training ML models and addressing various problems. (He et al., 2021; Consuegra-Ayala et al., 2022).
79 However, AutoML has not been widely applied in the fields of hydrology and disaster risk management,
80 and research has mainly focused on optimizing the integrated model to achieve better performance
81 (Özdemir et al., 2023). Continuous research has highlighted the potential role of AutoML in flood risk
82 detection and assessment (Guo et al., 2022; Vincent et al., 2023; Munim et al., 2024). Guo et al. (2022)
83 compared AutoML with three single ML algorithms (CatBoost, XGBoost, and BPDNN) and concluded
84 that AutoML performed better in building rapid warning and comprehensive analysis models for urban
85 waterlogging. The model based on AutoML can be applied to areas without water level monitoring and
86 achieve accurate predictions and rapid warnings of waterlogging depth (Guo et al., 2022; Yan et al., 2024).
87 Abu-Salih et al. (2023) proposed a data-driven flood risk area detection model that combined the
88 integrated model with the AutoML tool and successfully solved the problems of data balance and strategy
89 modeling, while reducing the complexity of flood risk area prediction. Previous studies have provided
90 a theoretical basis and scientific reference for the application of AutoML methods to flood risk



91 assessment. However, the use of AutoML for research purposes is a complex issue, and many new
92 opportunities and challenges remain regarding its specific applications.

93 Although AutoML can objectively and efficiently calculate flood risk, it lacks comprehensiveness and
94 judgment. Therefore, when evaluating the indicators of various dimensions of flood risk, quantifying the
95 impacts of different levels of each indicator on flood risk is impossible, and determining the indicator
96 weight is challenging. Therefore, to determine the indicator weight, using relevant statistical methods is
97 necessary. Multicriteria decision analysis (MCDA) is a useful tool for considering complex decision-
98 making problems in flood risk management(Fernández and Lutz, 2010). The analytic hierarchy process
99 (AHP) is one of the most popular MCDA techniques(Donegan et al., 1992). This technique emphasizes
100 the importance of the subjective judgment of decision makers and the consistency of pairwise
101 comparisons of standards in the decision-making process (Saaty, 1980). Recent studies have focused on
102 integrated frameworks of ML models and MCDA technology for flood hazard assessment (Kanani-Sadat
103 et al., 2019; Khosravi et al., 2019; Gudiyangada Nachappa et al., 2020; Mia et al., 2023). However,
104 research focusing on using an integrated framework of AutoML and AHP techniques is still limited.

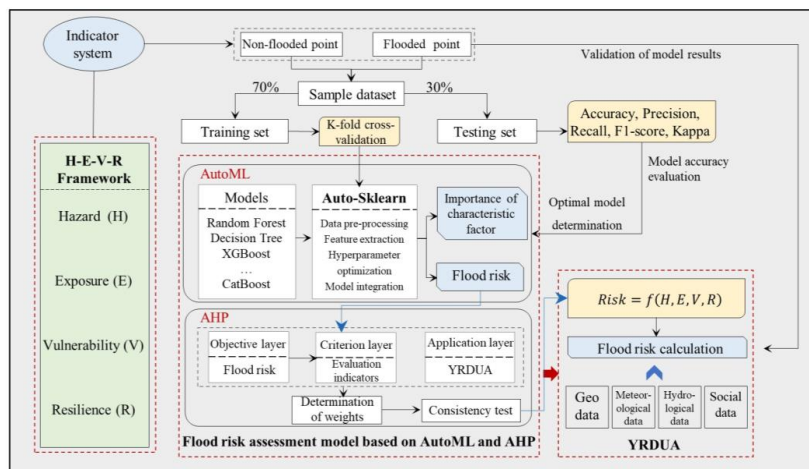
105 This study constructs a flood risk assessment model based on AutoML and AHP by examining the factors
106 influencing flood risk in the YRDUA. Based on the proposed flood risk assessment model, the risk,
107 exposure, vulnerability, and resilience as well as their corresponding weights of flooding in the YRDUA
108 are calculated, and the regional flood risk level zoning map is obtained. Comparative analysis of the
109 superimposed flooded points data reveals that the distribution of flooded points in the study area is
110 basically consistent with the distribution of high and medium-to-high risk areas of flooding. The
111 proportion of quantifying the distribution is 87.45%, indicating that the model in this paper performs well
112 and has high credibility for flood risk assessment. The analysis of spatial and temporal patterns of flood
113 risk change over the past 30 years provides scientific basis and theoretical support for disaster prevention
114 and mitigation in the YRDUA.

115 **2 Materials and methods**

116 In this section, the study area is briefly introduced (Section 2.1), and each individual component of the
117 study is further discussed along with the basic geographic information, meteorology, social statistics,
118 historical disaster data, and other fields involved in the study of urban agglomeration flood disasters and



119 their risks (Section 2.2). The framework of the flood risk assessment model is shown in **Figure 1**. The
120 factors influencing flood risk in the YRDUA are explored, and a flood risk assessment index system is
121 established (Section 2.3). The optimal model in AutoML is selected to calculate the importance of flood
122 hazard and hazard characteristic factors (Section 2.4), and the model is combined with AHP to determine
123 the weight of each risk indicator (Section 2.5). Ultimately, a flood risk assessment model based on
124 AutoML and AHP is constructed.



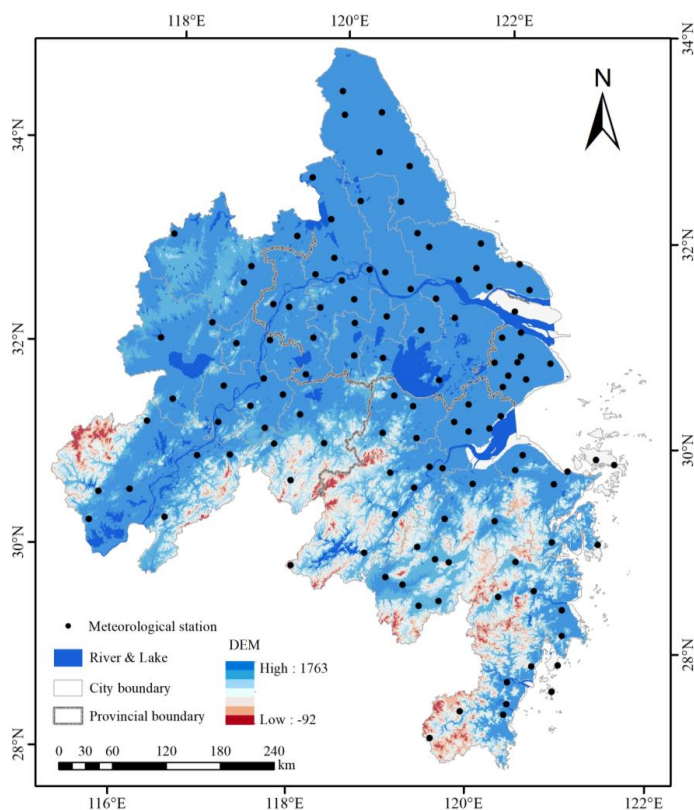
125
126 **Figure 1: Flood risk assessment modeling framework.**
127

128 2.1 Study area

129 The Yangtze River Delta Urban Agglomeration, located in the eastern coastal region of China(27° 04′–
130 34° 49′ N; 115° 75′–122° 95′ E), includes 27 cities: 8 in Anhui Province, 9 in Jiangsu Province, 9 in
131 Zhejiang Province, and Shanghai(Figure 2)(Yang et al., 2024). Influenced by the East Asian summer
132 monsoon, the study area features low-lying plains in the northern region and higher hilly terrain in the
133 southern region, along with numerous waterways(Ding et al., 2021). With the recent accelerated climate
134 change and urbanization, extreme precipitation events in the Yangtze River Delta (YRD) have been
135 occurring ever more frequently, and the temporal and spatial distribution differences in precipitation have
136 increased. Additionally, the increase in impervious surfaces, narrow plains rivers, and poor drainage may
137 result in more frequent and widespread urban flooding and waterlogging disasters (Wan et al., 2013).
138 This region is economically developed and densely populated , making it the largest urban agglomeration
139 in Asia(Sun et al., 2023). In 2008, the Gross Domestic Product (GDP) of the YRD accounted for 17.5%



140 of the GDP of the entire country, i.e., 4.3 trillion yuan, and the per capita GDP was 44,468 yuan, i.e.,
141 twice the national average level. The population has reached 97.2 million, i.e., 7.3% of China's total
142 population, and the region's average population density is 877 persons/km², i.e., approximately twice the
143 national average (Gu et al., 2011). Therefore, the potential risks of flood and waterlogging disasters are
144 substantial.



145
146 **Figure 2: Study area.**

147
148 **2.2 Data sources**

149 The study of flood disasters and their associated risks in urban agglomerations involves complex natural
150 and social factors. Therefore, we collected and preprocessed data from multiple fields, such as basic
151 geography, meteorology, social statistics, and historical disasters. **Table 1** lists the data types and



152 resolutions collected for the research area.

153 **Table 1: Data sources.**

Dataset	Data name	Spatial resolution	Data source
Basic geographic information data	Basic geographic information data	Vector data	Resources and Environmental Science and Data Center, Chinese Academy of Sciences (https://www.resdc.cn/)
	Digital elevation model	30 m	The U.S. geological survey (https://earthexplorer.usgs.gov/)
	River network density data	Vector data	Resources and Environmental Science and Data Center, Chinese Academy of Sciences (https://www.resdc.cn/)
	Land use data	30 m	Wuhan University CLCD dataset (https://zenodo.org/records/8176941)
Basic geographic information data	Normalized difference vegetation index data	30 m	National Science and Technology Infrastructure - National Ecosystem science Data Center (http://www.nesdc.org.cn)
	Building data	Vector data	OpenStreetMap (https://openstreetmap.maps.arcgis.com/)
Meteorological data	Precipitation data	Site data	National Meteorological Information Center, China Meteorological Administration
Social statistics	Population data	Prefecture-level	Provincial and municipal statistical yearbooks and bulletins
	Gross domestic product	Prefecture-level	Provincial and municipal statistical yearbooks and bulletins
	Unemployment figures	Prefecture-level	Provincial and municipal statistical yearbooks and bulletins
	Health care statistics	Prefecture-level	Provincial and municipal statistical yearbooks and bulletins
Historical disaster data	Historical flooding data	250 m	Global Flood Database
	Historical flood hazard data	The statistics	EM-DAT database (https://www.emdat.be/)

154

155 **2.3 Establishment of an flood risk assessment indicator system**

156 Although risk is a universal concept, it has no universal definition (Aven, 2016; Mishra and Sinha, 2020).

157 Based on the hazard–exposure–vulnerability (H–E–V) disaster risk framework, we considered the

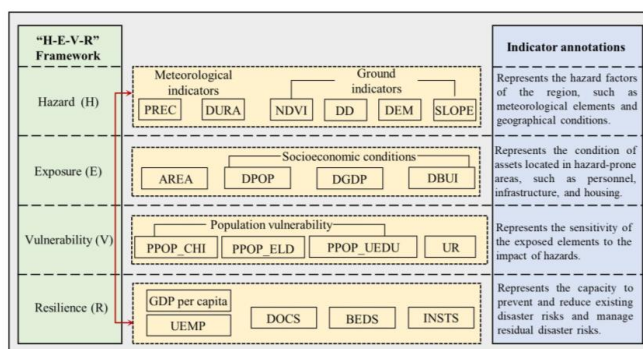


158 particularity of flood risk research at the urban agglomeration scale, incorporated resilience indicators
159 into the existing framework, and constructed a four-dimensional flood risk assessment framework of
160 hazard–exposure–vulnerability–resilience (H–E–V–R) that can assess regional flood risks more
161 comprehensively and systematically. The conceptual description of flood risk in this study can be
162 expressed in the Eq. (1):

$$163 \quad Risk = f(H, E, V, R) = \sum_{i=1}^a \omega_H H_i + \sum_{i=1}^b \omega_E E_i + \sum_{i=1}^c \omega_V V_i + \sum_{i=1}^d \omega_R R_i, \quad (1)$$

164 where H , E , V , and R represent the danger of, exposure to, vulnerability to, and resilience in response
165 to floods, respectively; ω_H , ω_E , ω_V , and ω_R are the weights of danger, exposure, vulnerability, and
166 resilience, respectively; H_i , E_i , V_i , and R_i are the values of items i of the indicators, respectively; and
167 a , b , c , and d are the numbers of the indicators, respectively.

168 We constructed a flood risk assessment index system for the YRDUA based on the “H–E–V–R”
169 framework, the actual situation of the study area, the formation mechanisms of flood disasters, and the
170 findings of relevant studies (Gain et al., 2015; Criado et al., 2019; Hsiao et al., 2021). We selected four
171 first-level indicators (i.e., hazard, exposure, vulnerability, and resilience indices) and 19 second-level
172 indicators: Average annual precipitation (PREC), Annual Cumulative Heavy Rainfall Duration (DURA),
173 Digital Elevation Model (DEM), SLOPE, Drainage Density (DD), and Normalized Difference
174 Vegetation Index (NDVI) were selected as hazard indicators to evaluate the sensitivity of flood-prone
175 environments; land area (AREA), Population Density (DPOP), GDP Density (DGDP), and Building
176 Density (DBUI) were selected as exposure indicators to measure the degree of exposure of the natural
177 environment or social system to flooding; Proportion of Child Population (PPOP_CHI), Proportion of
178 Elderly Population (PPOP_ELD), Proportion of Uneducated Population (PPOP_UEDU), and
179 Urbanization Rate (UR) were selected as vulnerability indicators to reflect the vulnerability to flooding;
180 GDP per capita, Unemployment Rate (UEMP), Number of Doctors (DOCS), Number of Medical
181 Institutions (INSTS), and Number of Hospital Beds (BEDS) were selected as resilience indicators. A
182 detailed description of the flood risk assessment index system is presented in **Figure 3**.



183 **Figure 3: Flood risk assessment index system for the YRDU based on the H–E–V–R framework.**

184

185 2.4 Flood risk calculation method based on AutoML

186 2.4.1 Feature selection

187 The training sample dataset was generated based on flooded and non-flooded points in the study area.

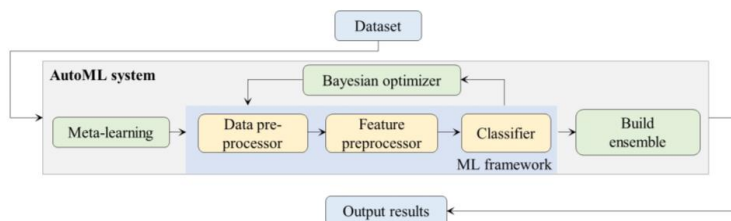
188 The main factors affecting flood risk were considered during input feature selection. Rainfall and
 189 rainstorms are important factors that lead to floods, and flooding is closely related to topography, slope,
 190 vegetation cover, and hydrological conditions. Therefore, six indicator factors, namely PREC, DURA,
 191 DEM, SLOPE, NDVI, and DD, were selected as the input features of the model. To verify the model,
 192 70% of the data in the sample were set as the training dataset and the remaining 30% of the data were set
 193 as the testing dataset through random sampling.

194 When the number of samples is small, data balancing is essential to ensure uniform sampling and reduce
 195 the deviations among the training, validation, and original datasets. Data balancing refers to the process
 196 of achieving a balanced distribution of data for each labeled category; it is particularly important when
 197 the number of observations in each class is significantly different. One way to address an imbalanced
 198 dataset is to oversample the minority classes. In this study, we assessed flood risk based on the
 199 identification of flooded point in the sample, which is essentially a binary classification problem;
 200 therefore, the output features are 0, i.e., negative categories (non-flooded points), versus 1, i.e., positive
 201 categories (flooded points). The processed dataset comprised 278 positive samples (flooded points) and
 202 278 negative samples (non-flooded point).



203 2.4.2 Model training and hyperparameter optimization

204 Training samples were generated using the data from flooded and non-flooded points in the study area,
205 and the Auto-Sklearn was used for model training, its principle is shown in **Figure 4**. The Auto-sklearn
206 framework has multiple built-in machine learning algorithms. We selected 9 models that are more typical
207 or have better performance in flood hazard research: random forest (RF), extreme gradient boosting
208 (XGBoost), Light Gradient Boosting Machine (LightGBM), categorical feature boosting (CatBoost),
209 extra trees, decision tree, nearest neighbors, neural network, and linear. The training and testing datasets
210 were used to train the 9 machine learning models, and the hyperparameters were continuously adjusted
211 and optimized.



212
213 **Figure 4: Principles of Auto-Sklearn**

214
215 Hyperparameter optimization is an important step in ML model training. The aim of this step is to
216 determine a hyperparameter combination to generate a ML model that performs well on a specific dataset
217 and reduces the effect of the predefined loss function on a given dataset. In this study, we used a grid
218 search strategy for optimization. For each set of hyperparameter combinations, k-fold cross-validation
219 was used to evaluate the model and determine the hyperparameter combination of the optimal model that
220 achieved the highest prediction accuracy. Briefly, the training dataset was divided into K parts, of which
221 one was selected as the test set and the rest were used as the training set. The cross-validation was
222 repeated K times and the results were averaged K times. The model with the best average result among
223 all models was selected as the optimal model, and the final classification prediction result was the output.
224 In this study, we used 5-fold cross-validation.



225 2.4.3 Performance evaluation

226 To better compare the accuracy of the 14 selected ML models in the Auto-Sklearn framework for flood
227 risk assessment, multiple accuracy evaluation indicators were used to assess the test dataset. The
228 following combinations of the true category of the sample point and the category predicted by the
229 classifier were used: True Positive (TP)—the sample point is a flooded point, and the model classifier
230 also predicts that it is a flooded point; True Negative (TN)—the sample point is a non-flooded point, and
231 the model classifier also predicts that it is a non-flooded point; False Positive (FP)—the sample point is
232 a flooded point, and the model classifier mistakenly predicts that it is a non-flooded point; False Negative
233 (FN)—the sample point is a non-flooded point, and the model classifier mistakenly predicts that it is a
234 flooded point. Therefore, four related indicators were selected: Accuracy, Precision, Recall and F1-score,
235 and the consistency metric kappa coefficient, the calculation formula is as follows Eq. (2), Eq. (3), Eq.
236 (4), Eq. (5), Eq. (6). A combination of multiple indicators can be used to better compare the
237 performances of several models in the Auto-Sklearn framework for flood point identification and flood
238 risk assessment. The equations for calculating the above indicators are shown below. The most intuitive
239 precision performance indicator is accuracy. As the Auto-Sklearn framework uses data balancing to
240 ensure adaptive balanced class distribution, the model with the highest accuracy value is the best
241 performing model in flood point identification in this study.

$$242 \text{ Accuracy} = \frac{TP+TN}{TP+FP+TN+FN}, \quad (2)$$

$$243 \text{ Precision} = \frac{TP}{TP+FP}, \quad (3)$$

$$244 \text{ Recall} = \frac{TP}{TP+FN}, \quad (4)$$

$$245 \text{ F1 - score} = \frac{2TP}{2TP+FP+FN}, \quad (5)$$

246 Among the indicators, *Accuracy* is determined based on the accuracy rate and can also be understood as
247 the consistency of the prediction, indicating the degree of closeness or distance between the predicted
248 category given by a set of data and its true category. Precision is the accuracy rate and refers to the degree
249 of closeness or dispersion among the predicted categories. *Recall* is the recall rate and refers to the ability
250 of the prediction result to correctly classify and identify the flooded points. F1-score is the harmonic



251 mean of Precision and Recall and is equivalent to the comprehensive evaluation index of the precision
252 and recall rates and can better reflect the recognition performance of the model.

253 Kappa is an indicator of consistency in statistics, it is used to measure the effects of classification, and it
254 was calculated based on the confusion matrix of the true and predicted categories in this study. Its value
255 range is [-1, 1]. A model with a low Kappa value indicates an unbalanced confusion matrix. Its formula
256 is as Eq. (6), Eq. (7).

$$257 \quad Kappa = \frac{Accuracy - P_e}{1 - P_e}, \quad (6)$$

$$258 \quad P_e = \frac{(TP+FP)+(TP+FN)+(TN+FN)+(TN+FP)}{(TP+FP+TN+FN)^2}, \quad (7)$$

259 where P_e represents the accidental consistency.

260 **2.5 Method for determining flood risk index weights based on AHP**

261 **2.5.1 Establishing a hierarchical model**

262 According to the decision-making objectives, factors, and applications in decision-making problems, the
263 AHP can be divided from bottom to top into the target, criterion, and application layers. Among them,
264 the target layer is the problem to be solved (i.e., final flood risk). The criterion layer is the intermediate
265 link, including the factors to be considered and the decision making criteria. The factors can be divided
266 into different evaluation indicators, including four first-level indicators (danger, exposure, vulnerability,
267 and resilience) and their corresponding 19 second-level indicators. The criterion layer comprises various
268 weight combination schemes linked to the target layer. The application layer is the final optional scheme
269 and specific application of the decision. The final weight scheme and evaluation results of this study
270 were applied to the YRDUA.

271 **2.5.2 Constructing the judgment matrix**

272 After the hierarchical structure was established, a judgment matrix was constructed based on the
273 relationship between the criteria and indicators. Different elements in the sublevel were compared
274 pairwise, and the relative importances of all elements in the current layer and previous layer were
275 compared. Typically, a pairwise comparison matrix is used as representative. In this study, we adopted
276 the 1–9 scale method as the importance measurement standard. The importance comparison relationship



277 is presented in **Table 2**, where the matrix element a_{ij} represents the comparison result of the i th element
 278 relative to the j th element.

279 **Table 2: Pairwise comparison point-based rating scale of AHP.**

Ranking	Importance Level
1	Equally important
3	i is slightly more important than j
5	i is much more important than j
7	i is very much more important than j
9	i is extremely important than j
2, 4, 6, 8	Intermediate value of two adjacent judgements
Reciprocal	Comparative judgement of j vs., $a_{ji} = 1/a_{ij}$

280

281 2.5.3 Solving the eigenvector of the judgment matrix

282 Based on the judgment matrix, the square root method was used to solve the eigenvector and eigenroot.
 283 The first step is to calculate the square root a_{ij} of the product of each row of the judgment matrix n ,
 284 then normalize it, and finally calculate the maximum eigenroot of the judgment matrix. The formula is
 285 as Eq. (8), Eq. (9), Eq. (10).

$$286 \quad M_i = \sqrt[n]{\prod_{j=1}^n a_{ij}}, \quad (8)$$

$$287 \quad W_i = \frac{M_i}{\sum_{i=1}^n M_i}, \quad (9)$$

$$288 \quad \lambda_{max} = \sum_{i=1}^n \frac{(AW)_i}{nW_i}, \quad (10)$$

289 2.5.4 Consistency check

290 After the eigenvector calculation is completed, a consistency test is required to reduce the subjectivity in
 291 the judgment matrix and enhance the scientific nature of the data and calculations. The consistency
 292 indicator (CI) is used to measure the deviation of the judgment matrix from the consistency: the smaller
 293 the CI, the greater the consistency of the judgment matrix. When $CI = 0$, the judgment matrix is
 294 completely consistent. The CI calculation formula is as Eq. (11).

$$295 \quad CI = \frac{\lambda - n}{n - 1}, \quad (11)$$



296 To quantify the standard, the relative consistency (CR) index was further calculated as Eq. (12).

$$297 \quad CR = \frac{CI}{RI}, \quad (12)$$

298 where average Random Consistency Index (RI) represents the average random consistency, which is only
299 related to the order of the judgment matrix. The RI values of judgment matrices of order Table 3:Table
300 3.

301 **Table 3: Consistency index (RI) for a randomly generated matrix.**

n	1	2	3	4	5	6	7	8	9	10
RI	0.00	0.00	0.52	0.89	1.12	1.26	1.36	1.41	1.46	1.49

302

303 CR was determined based on the RI value. When $CR < 0.1$, the consistency of the judgment matrix is
304 considered good. When $CR > 0.1$, the consistency of the judgment matrix is unacceptable, and the
305 judgment matrix must be adjusted and modified. In such cases, the corresponding judgment matrix was
306 further constructed, and the eigenvector and eigenroot were calculated using the following formulas:
307 Finally, the judgment matrix that passed the consistency test was used to calculate the weights of the
308 indicators at the different levels.

309 **3 Results and discussion**

310 **3.1 Model flood risk results and evaluation**

311 **3.1.1 AutoML optimal model selection**

312 In the experiment, 9 typical ML models under the Auto-Sklearn framework were used to process the
313 sample dataset, with 70% of the sample set being used as the training dataset and 30% being used as the
314 testing dataset. The results of the comparative analysis of the model performance based on the test dataset
315 are presented in **Table 4**. A comprehensive analysis of the results revealed that the accuracy of the models
316 followed the order of CatBoost (0.8960) = LightGBM (0.8960) > Extra Trees (0.8880) > other models >
317 Nearest Neighbors. In terms of the precision index, CatBoost had the highest value (0.9030), followed
318 by those of LightGBM (0.8960) and Extra Trees (0.8893). Meanwhile, CatBoost had the highest recall
319 rate of 0.8883, followed by that of Extra Trees at 0.8870. The F1-score and Kappa coefficient of the
320 CatBoost model were also markedly higher than those of the other models, reflecting the model's good
321 consistency. A comprehensive comparison showed that the accuracy, precision, F1-score, and kappa



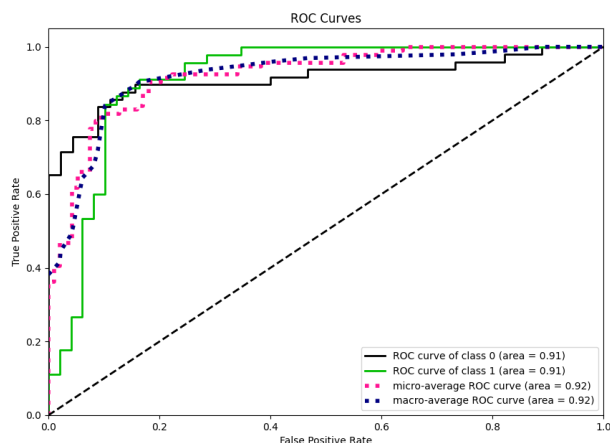
322 coefficient of the CatBoost model were the highest, with its accuracy reaching 0.8960, indicating that the
323 recognition and prediction accuracy of the flooded points in the study area based on the CatBoost model
324 were obviously better than those of other common machine learning models. Since flood data often
325 involve various environmental factors and complex interactions, the CatBoost model is highly effective
326 at handling these intricate nonlinear relationships and feature interactions. Additionally, the model
327 incorporates multiple regularization mechanisms during tree construction, which helps prevent
328 overfitting and enhances the model's generalization capability.

329 **Table 4: Comparative analysis of the performances of different ML models.**

Models	Accuracy	Precision	Recall	F1-score	Kappa
CatBoost	0.8960	0.9030	0.8883	0.8960	0.7915
XGBoost	0.8640	0.8748	0.8640	0.8624	0.7256
LightGBM	0.8960	0.8960	0.7890	0.8015	0.7324
Random Forest	0.8320	0.8482	0.8320	0.8309	0.6662
Extra Trees	0.8880	0.8893	0.8870	0.8877	0.7751
Decision Tree	0.8720	0.8810	0.8720	0.8708	0.7419
Linear	0.8480	0.8682	0.8480	0.8450	0.6926
Nearest Neighbors	0.7440	0.7747	0.7440	0.7390	0.4937
Neural Network	0.8480	0.8682	0.8480	0.8450	0.6926

330

331 By comparing the performances of the 9 models, we found that the CatBoost model was more effective
332 in identifying flooded points. To further verify the excellent performance of the model, the receiver
333 operating characteristic (ROC) curve and area enclosed by the coordinate axes (corresponding area under
334 the curve [AUC] value) were plotted based on the test dataset to determine the accuracy of the model's
335 binary classification effect: the larger the AUC value, the more accurate the model prediction. When
336 $AUC > 0.8$, the model prediction effect is very good (Sinha et al., 2008). The verification results are
337 shown in **Figure 5**. The AUC value of the CatBoost model reached 0.91, guaranteeing the performance
338 and prediction reliability of the CatBoost model. Based on this, the CatBoost model was selected to
339 calculate the flood risk in the YRDUA.



340

341 **Figure 5: Receiver operating characteristic (ROC) curves and corresponding area under the curve (AUC)**
342 **values of the CatBoost model.**

343

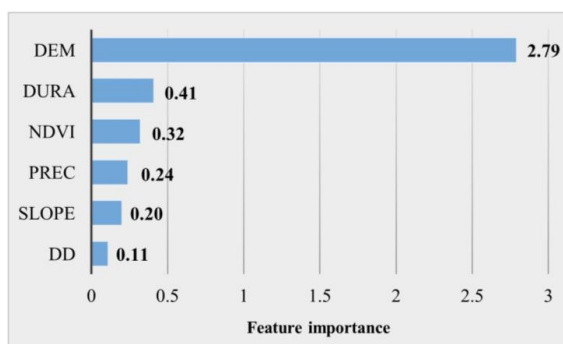
344 3.1.2 Analysis of hazard factors

345 (1) Ranking of importance

346 Among the six characteristic factors affecting flood risk, in order to clarify the main factors affecting
347 flood risk in the YRDUA, this study quantifies the degree of importance of each risk indicator factor
348 through the CatBoost model, and its importance ranking is shown in **Figure 6**. The results indicated that
349 there are obvious differences in the degree of influence of the indicators on flood risk within the study
350 area. DEM is the primary factor affecting flood risk, with an importance level of 68.55%, which far
351 exceeds the other factors, which is also in line with the findings of many researchers within the
352 region (Mei et al., 2021; Wan et al., 2013). Analyzing the main reasons, compared to higher terrain areas,
353 low-lying and relatively flat depressions become natural catchment areas. Additionally, since the main
354 urban areas of the YRDUA predominantly consist of impervious surfaces, the surface runoff formed is
355 difficult to infiltrate, further exacerbating the risk of water accumulation and flooding in low-lying areas.
356 At the same time, although rainfall is the primary disaster-causing factor for storm-induced flooding, the



357 importance of the PREC is relatively low. Instead, the factor representing the DURA contributes 10.07%
358 to the flood risk. This indicates that extreme weather events leading to heavy rainfall are more likely to
359 cause considerable flood hazards.



360
361 **Figure 6: Importance Ranking of Hazard Factors Based on the CatBoost Model**

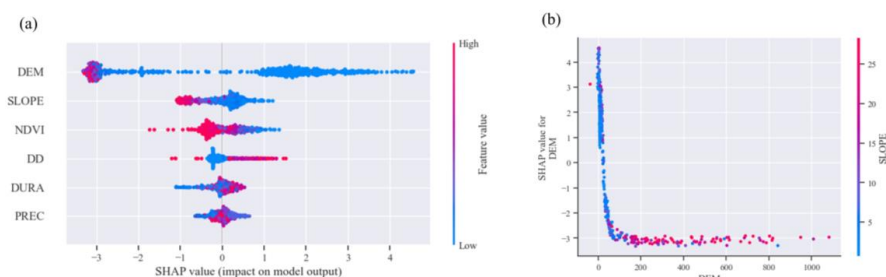
362

363 (2) SHAP interpretability analysis

364 To further analyze the interpretability of the model and understand the impact of individual flood hazard
365 indicators on the model's classification results, this paper calculates Shapley Additive Explanations
366 (SHAP) to indicate the contribution of each feature in the sample (Lundberg and Lee, 2017). SHAP is a
367 post-hoc interpretability method for models. Its core idea is to calculate the marginal contribution of
368 features to the model's output (Wang et al., 2023a). For each prediction sample, the model produces a
369 predicted value. The SHAP value is the value assigned to each feature in the sample, thereby determining
370 the contribution and explaining the model. **Figure 7(a)** shows the scatter plot generated by SHAP in the
371 training set, which can be analyzed in conjunction with the connotations and significance of flood hazard
372 characteristic factors. In the **Figure 7(a)**, each row represents a feature, and the horizontal axis is the
373 SHAP value. The features are ranked according to the average absolute value of SHAP, which can be
374 understood as the most important features. The wider areas indicate a large concentration of samples.



375 Each point represents a sample, with redder colors indicating higher feature values and bluer colors
376 indicating lower feature values. The results indicate that for risk features, DEM, SLOPE, and NDVI have
377 varying degrees of negative impact on flood risk, while DD, annual DURA, and PREC have varying
378 degrees of positive impact on flood risk. This indicates that the higher DEM, the steeper SLOPE, and the
379 greater the vegetation cover, the lower the flood hazard in the area. Conversely, higher DD, DURA, and
380 higher PREC increase the flood hazard. At the same time, the absolute value of DEM is the highest, with
381 SHAP values showing pronounced clustering below zero and a relatively dispersed sample distribution,
382 indicating that the elevation factor is the most hazard factor affecting flooding.



383
384 **Figure 7: (a) Scatter Plot of Hazard Indicators from SHAP Analysis. (b) SHAP Dual Dependence Analysis of**
385 **Elevation and Slope Factors.**

386
387 To directly capture the interaction effects between paired indicator factors, this study used SHAP
388 interaction values based on game theory, ensuring consistency while also explaining the interaction
389 effects of individual predictions. For the DEM feature, which had the highest importance in the SHAP
390 analysis, the factor most strongly correlated with it was SLOPE. Therefore, to illustrate how one feature
391 interacts with another to affect the model training results, this study used DEM and SLOPE as examples
392 to plot the SHAP interaction scatter plot, representing the dependency of the DEM feature. The results
393 are shown in **Figure 7(b)** This dependency plot takes the form of a logarithmic function, indicating that



394 as DEM increases, the flood hazard decreases. Additionally, the slope has a negative effect on the flood
 395 hazard in relation to elevation; that is, at lower elevations and gentler slopes, the flood hazard is greater.

396 3.1.3 Determination of flood risk index weights

397 A judgment matrix was constructed for 19 indicator factors. A hazard index was constructed based on
 398 feature importance calculated using AutoML. The exposure, vulnerability, and resilience indicators were
 399 determined based on existing literature and relevant expert scores (Hsiao et al., 2021). Combined with
 400 the actual characteristics of the YRDUA, the 1–9 scale method was used to compare item-by-item any
 401 two indicators and determine their relative importances and assign weights. Finally, the judgment matrix
 402 results were tested for consistency, and the CR value was 0.0058, i.e., $\ll 0.100$, indicating that the results
 403 passed the consistency test and that the flood risk index weight values calculated using the AHP were
 404 acceptable. The specific indicator weights and attribute representations of flood risk are shown in **Table**
 405 **5**.

406 **Table 5: Flood risk index weights.**

Dimension	Indicator	Unit	Attribute	Weight
Hazard (0.4798)	PREC	mm	+	4%
	DURA	Day	+	10.8%
	NDVI		-	7.6%
	DEM	km	-	22.99%
	SLOPE	°	-	6.4%
	DD	km/km ²	+	3.2%
Exposure (0.1083)	AREA	km ²	+	1.1%
	DPOP	people/km ²	+	4.32%
	DGDP	10,000 yuan/km ²	+	3.84%
	DBUI	km ²	+	1.16%
Vulnerability (0.1312)	PPOP_CHI	%	+	4.92%
	PPOP_ELD	%	+	3.04%
	PPOP_UEDU	%	+	2.11%
Resilience (0.2807)	UR	%	-	2.05%
	GDP per capita	100 million yuan/10,000 People	-	4.43%



Dimension	Indicator	Unit	Attribute	Weight
	UEMP	%	+	5.04%
	DOCS	Per person	-	4.13%
	INSTS	Each	-	0.45%
	BEDS	Per bed	-	6.28%

407

408 The weighted results reflect the degrees of influence of the different indicator factors on flood risk.
409 Danger was the decisive factor affecting flood risk, with a weight of 0.4798, followed by resilience and
410 vulnerability. Exposure had a relatively low impact on flood risk. In terms of danger, the topography and
411 DURA were the main factors affecting the occurrence of flooding. These two indicators determined the
412 characteristics of flood disasters in the YRDUA from the perspective of disaster-prone environments and
413 driving factors, respectively. In terms of exposure, the YRDUA is a typical area with rapid social,
414 economic, and population growths in China. High population and GDP densities increase the risk of
415 flood exposure. In addition, the uneven age distribution and education levels of the population are
416 important social factors affecting the risk of flood disasters in urban agglomerations. In terms of
417 resilience, improving health and medical infrastructure, developing the regional economy, and reducing
418 unemployment rates are conducive to improving the overall disaster response capacity of the region and
419 reducing the risk of flood disasters in the YRDUA.

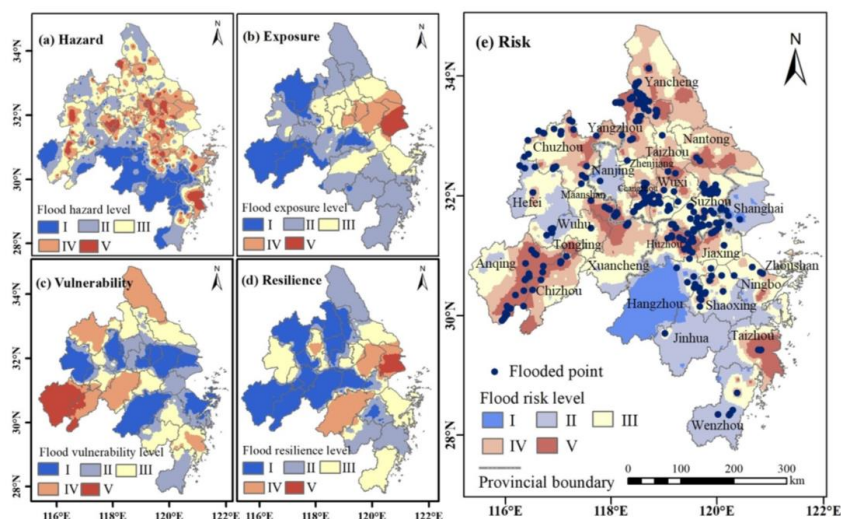
420 **3.1.4 Model results verification**

421 Based on AutoML and AHP, the levels of danger, exposure, vulnerability, and resilience were calculated
422 for floods in the YRDUA and the spatial distribution of flood risks in the region was obtained according
423 to the weights determined by the model. Combined with the natural breakpoint classification method, a
424 flood risk zoning map of the YRDUA was constructed. The extracted flood points were superimposed
425 on the map to verify whether the model exhibited good flood risk assessment capabilities. The results are
426 shown in **Figure 8**, indicating that the distribution of flood points was consistent with the distribution of
427 high and medium-to-high risk areas in the region, with the model assessment results corresponding well
428 with the actual flooding situation. To specifically illustrate the correspondence of the results, the
429 proportion of flood points distributed in high and medium-to-high risk areas was quantitatively calculated.



430 The obtained value was 87.45%, indicating that the flood risk assessment results of the model in this
431 study were highly credible, and subsequent analysis could be conducted.

432 As shown in **Figure 8**, the high and medium-to-high risk areas in the YRDUA were mainly located in the
433 northern part of the region, concentrated in Chizhou, Anqing, Ma'anshan, and Xuancheng Cities in Anhui
434 Province, Yancheng and Yangzhou Cities in Jiangsu Province, and Taizhou City in Zhejiang Province.
435 Meanwhile, most areas of Hangzhou City had the lowest risk. The flood risks in cities such as Shanghai,
436 Nanjing, and Jinhua were also relatively low. The overall analysis showed that the flood risk in the study
437 area was low in the southwest and high in the northeast, determined largely by natural terrain and
438 meteorological factors. The spatial distribution of the flood hazard class was similar to the distribution
439 of flood risks; exposure decreased stepwise from Shanghai to the surrounding areas, reflecting that
440 densely populated and economically developed cities have higher exposure. Areas with higher
441 vulnerability were mainly concentrated in Chizhou, Anqing, Xuancheng, Chuzhou, and Yancheng Cities.
442 The number of vulnerable people in these cities was relatively high. Vulnerability has aggravated the
443 flood risks in Chizhou and Anqing Cities on the basis of flood risk. Meanwhile, Shanghai had the best
444 resilience performance, followed by those of Hangzhou, Suzhou, and Nanjing Cities, greatly lessening
445 the flood risks in these cities.

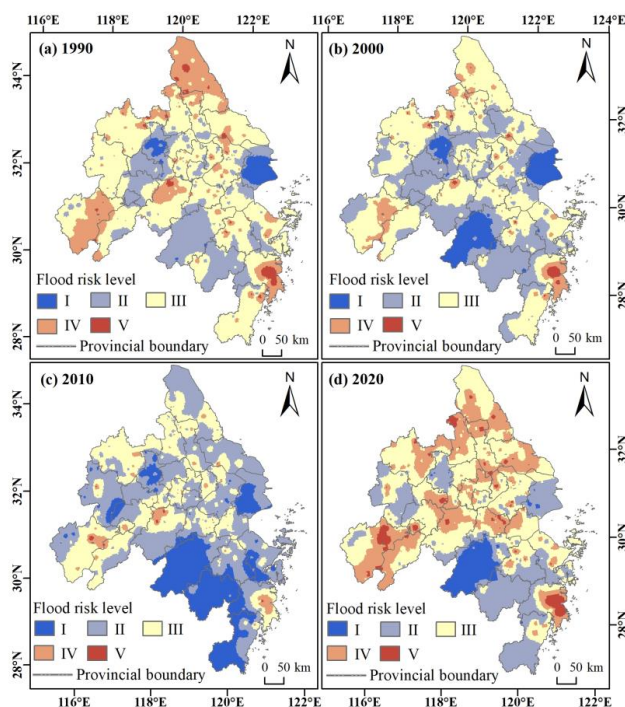


446
447 **Figure 8: Flood risk level distribution and verification results based on a flood risk assessment model.**
448

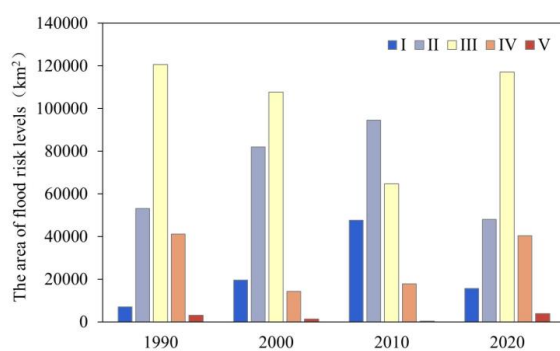


449 3.2 Analysis of changes in the spatiotemporal characteristics of flood risk

450 The flood risk results for the YRDUA from 1990 to 2020 were obtained based on the flood risk
451 assessment model proposed in this study. As the interannual difference in flood risk in the region was
452 small and the change response was weak, we selected the flood risk results for 1990, 2000, 2010, and
453 2020 to analyze the changes in the spatiotemporal pattern. Regarding spatial patterns (**Figure 9**), the flood
454 risk in the YRDUA showed clear spatial heterogeneity. The southwestern part of the study area and
455 Shanghai have shown low flood risks over the past 30 years, whereas the central and northern parts of
456 the region have been more likely to face flood risks depending on the natural conditions, population,
457 economic conditions, and recovery capacity of the region. Regarding temporal patterns, from 1990 to
458 2010, areas with high and medium-to-high risk decreased markedly. By 2010, most of the YRDUA
459 (except for a few areas) was in a state of medium risk or below, with the southwestern region exhibiting
460 a large range of low risk levels. The corresponding areas for each risk level are shown in **Figure 10**. From
461 1990 to 2010, areas of low and low-to-medium risk levels gradually increased, maximizing in 2010,
462 whereas areas of medium risk and above continued to decrease. By 2020, the number of high risk areas
463 for flooding increased. There is a tendency for areas of medium-to-high risk in the central region to shift
464 towards high risk areas in 2020, as compared to the state in 1990. Meanwhile, high risk areas for floods
465 also appeared in Chizhou and Anqing Cities in Anhui Province, which was mainly due to the
466 intensification of extreme weather, unbalanced population, and economic development in recent years.



467
 468 **Figure 9: Spatial distributions of flood risk in the YRDUA in different years during 1990–2020.**
 469



470
 471 **Figure 10: Areas at different levels of flood risk in the YRDUA in different years during 1990–2020.**
 472

473 To further analyze the changes in flood risk in the region, we calculated the change rate of the area of
 474 different risk levels every 10 years and the overall change rate over 30 years. The interannual rate of
 475 change was expressed in Eq. (13).

476
$$R_{i,j} = \frac{Risk_{i,j} - Risk_{i,i}}{Risk_{i,i}} \times 100\%, \quad (13)$$



477 where $R_{l,ij}$ is the rate of change of the flood risk area of a certain level l in a certain year, i and j are
478 different years, and $Risk_{l,i}$ and $Risk_{l,j}$ are the areas corresponding to the flood risk of this level in
479 different years.

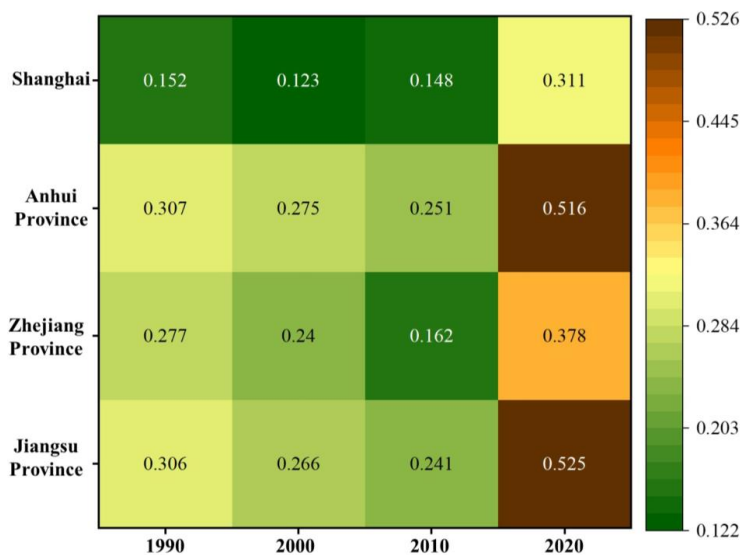
480 The interannual variation rate of the flood risk is shown in **Table 6**. Results showed that the interannual
481 variation between the areas of low and high risk was relatively large. The low risk area maximized in
482 2010, and both $R_{2000-1990}$ and $R_{2010-2000}$ showed a positive variation rate. The high risk area showed the
483 largest interannual variation rate from 2010 to 2020, reaching 12.218% and causing the high risk flood
484 area in 2020 to spread, resulting in a large high risk area.

485 **Table 6: Interannual change rates of flood risk areas of different levels.**

	$R_{2000-1990}$	$R_{2010-2000}$	$R_{2020-2010}$	$R_{2020-1990}$
I	1.766	1.443	-0.672	1.213
II	0.543	0.152	-0.491	-0.096
III	-0.106	-0.4	0.81	-0.029
IV	-0.653	0.252	1.254	-0.02
V	-0.528	-0.796	12.218	0.274

486

487 Analyzing the flood risk of the entire urban agglomeration does not reveal the spatial scale effect of flood
488 risk, nor does it consider the correlation and impact of flood risk at different spatial scales. To reflect the
489 distribution of and changes in flood risk at different spatial scales within the region, the risk intensity of
490 different provinces was further analyzed, and the results are shown in **Figure 11**, respectively. In **Figure**
491 **11**, the average flood risk reflects the differences in risk development of the provincial administrative
492 units in Shanghai, Anhui, Zhejiang, and Jiangsu in terms of time and space. Overall, all administrative
493 units in the YRDUA exhibited the highest flood risk in 2020, and the overall risk trend increased. At the
494 provincial level, Shanghai's flood risk was consistently low, showing a trend of first decreasing from
495 0.152 in 1990 to 0.123 in 2000 and then gradually increasing to 0.311 in 2020. Among the other three
496 provinces, Jiangsu and Anhui had relatively high flood risks, reaching 0.525 and 0.516, respectively, in
497 2020, whereas Zhejiang had a relatively low flood risk, which remained stable between 1990 and 2010,
498 with no distinct changes.



499

500 **Figure 11: Distribution of Average Flood Risk in Each Province of the Yangtze River Delta Urban**
501 **Agglomeration from 1990 to 2020**

502

503 **4 Conclusion**

504 Flood risk assessment at the scale of urban agglomeration is a hot research topic in the field of disaster
505 prevention and mitigation. In this study, the flood risk assessment indexes for YRDUA were determined
506 in different dimensions of danger, exposure, vulnerability and resilience, and a flood risk assessment
507 model based on AutoML and AHP was constructed to study the changes of spatial and temporal
508 characteristics of flood risk in the region in the last 30 years from 1990 to 2020, aiming to provide
509 scientific basis for the prevention and resilience of the YRDUA. The main conclusions of this study are
510 as follows:

511 (1) In the flood risk calculation, the CatBoost model has the highest Accuracy, Precision, F1-score, and
512 Kappa, and its Accuracy can reach 0.8960. Further analysis of the ROC curve and the corresponding
513 AUC value of the model shows that its AUC value is 0.91, which indicates that the CatBoost model has
514 the best performance and prediction reliability. Therefore, the CatBoost model was selected to calculate
515 the flood risk in the YRDUA.



516 (2) Using the flood risk assessment model based on AutoML and AHP to obtain the flood risk of the
517 YRDUA, superimposed on the flooded point data for comparative analysis, we found that the distribution
518 of flooded points in the study area is basically consistent with the distribution of high and medium-to-
519 high risk areas of flooding, and the proportion of the distribution of the quantification of its distribution
520 is 87.45%, which indicates that the model in this study has a good performance and credibility regarding
521 the assessment of flood risk.

522 (3) The spatial distribution of flood risk in the YRDUA during the 30-year study period shows obvious
523 heterogeneity, with the southwestern part of the region and Shanghai City having a low flood risk,
524 whereas the north-central part of the region faces a relatively high probability of flood risk. Between
525 1990 and 2010, there was a substantial decrease in the high and medium-to-high risk flood zones; yet by
526 2020, there was an increase in the high risk flood zones. There is a tendency for the medium-to-high risk
527 area in the center of the region to shift to a high risk area, whereas high risk areas also occur in the cities
528 of Chizhou and Anqing in Anhui Province.

529 (4) All administrative units of the YRD urban agglomeration exhibited the highest flood risk in 2020,
530 with an overall trend of increasing risk. At the provincial level, Jiangsu and Anhui Provinces possess
531 relatively high flood risks, whereas Zhejiang Province has a relatively low flood risk.

532 **Data availability.**

533 Data will be made available on request.

534 **Competing interests.**

535 The authors declare that they have no competing financial interests or personal relationships that may
536 have influenced the work reported in this study.

537 **Author contributions.**

538 **Yu Gao:** Writing - original draft preparation, Validation, Software, Methodology, Conceptualization

539 **Haipeng Lu:** Writing-review & editing, Visualization, Supervision, Formal analysis. **Yaru Zhang:**

540 Methodology, Formal analysis. **Hengxu Jin:** Writing - review & editing, Methodology. **Shuai Wu:**



541 Software, Formal analysis. **Yixuan Gao**: Visualization, Software. **Shuliang Zhang**: Writing-review &
542 editing, Resources, Project administration, Funding acquisition, Conceptualization .

543 **Acknowledgements**

544 This study was supported by the National Natural Science Foundation of China (Grant Nos. 42271483
545 and 42071364) and Jiangsu Provincial Natural Resources Science and Technology Project
546 (JSZRKJ202405). We would like to thank Editage (www.editage.cn) for English language editing.

547 **References**

- 548 Abu-Salih, B., Wongthongtham, P., Coutinho, K., Qaddoura, R., Alshaweesh, O., and Wedyan, M.: The
549 development of a road network flood risk detection model using optimised ensemble learning, *Eng. Appl.*
550 *Artif. Intell.*, 122, 106081, <https://doi.org/10.1016/j.engappai.2023.106081>, 2023.
- 551 Adnan, R. M., Yuan, X., Kisi, O., and Anam, R.: Improving Accuracy of River Flow Forecasting Using
552 LSSVR with Gravitational Search Algorithm, *Advances in Meteorology*, 2017, 1–23,
553 <https://doi.org/10.1155/2017/2391621>, 2017.
- 554 Anon: Identification of sensitivity indicators of urban rainstorm flood disasters: A case study in China,
555 *J. Hydrol.*, 599, 126393, <https://doi.org/10.1016/j.jhydrol.2021.126393>, 2021.
- 556 Aven, T.: Risk assessment and risk management: Review of recent advances on their foundation,
557 *European Journal of Operational Research*, 253, 1–13, <https://doi.org/10.1016/j.ejor.2015.12.023>, 2016.
- 558 Consuegra-Ayala, J. P., Gutiérrez, Y., Almeida-Cruz, Y., and Palomar, M.: Intelligent ensembling of
559 auto-ML system outputs for solving classification problems, *Inform. Sci.*, 609, 766–780,
560 <https://doi.org/10.1016/j.ins.2022.07.061>, 2022.
- 561 Criado, M., Martínez-Graña, A., San Román, J. S., and Santos-Francés, F.: Flood risk evaluation in urban
562 spaces: The study case of Tormes River (Salamanca, Spain), *International journal of environmental*
563 *research and public health*, 16, 5, 2019.
- 564 Ding, T., Chen, J., Fang, Z., and Chen, J.: Assessment of coordinative relationship between
565 comprehensive ecosystem service and urbanization: A case study of Yangtze River Delta urban
566 Agglomerations, China, *Ecol. Indic.*, 133, 108454, <https://doi.org/10.1016/j.ecolind.2021.108454>, 2021.



- 567 Donegan, H. A., Dodd, F. J., and McMaster, T. B. M.: A New Approach to Ahp Decision-Making,
568 Journal of the Royal Statistical Society: Series D (The Statistician), 41, 295–302,
569 <https://doi.org/10.2307/2348551>, 1992.
- 570 Echendu, A. J.: The impact of flooding on Nigeria’s sustainable development goals (SDGs), Ecosyst.
571 Health Sustainability, 6, 1791735, <https://doi.org/10.1080/20964129.2020.1791735>, 2020.
- 572 Fabian, P.: Scikit-learn: Machine learning in Python, Journal of machine learning research 12, 2825,
573 2011.
- 574 Fernández, D. S. and Lutz, M. A.: Urban flood hazard zoning in Tucumán Province, Argentina, using
575 GIS and multicriteria decision analysis, Eng. Geol., 111, 90–98, 2010.
- 576 Gain, A. K., Mojtahed, V., Biscaro, C., Balbi, S., and Giupponi, C.: An integrated approach of flood risk
577 assessment in the eastern part of Dhaka City, Nat. Hazards, 79, 1499–1530,
578 <https://doi.org/10.1007/s11069-015-1911-7>, 2015.
- 579 Gu, C., Hu, L., Zhang, X., Wang, X., and Guo, J.: Climate change and urbanization in the Yangtze River
580 Delta, Habitat Int., 35, 544–552, <https://doi.org/10.1016/j.habitatint.2011.03.002>, 2011.
- 581 Guan, X., Yu, F., Xu, H., Li, C., and Guan, Y.: Flood risk assessment of urban metro system using
582 random forest algorithm and triangular fuzzy number based analytical hierarchy process approach,
583 Sustainable Cities and Society, 109, 105546, <https://doi.org/10.1016/j.scs.2024.105546>, 2024.
- 584 Gudiyangada Nachappa, T., Tavakkoli Piralilou, S., Gholamnia, K., Ghorbanzadeh, O., Rahmati, O., and
585 Blaschke, T.: Flood susceptibility mapping with machine learning, multi-criteria decision analysis and
586 ensemble using Dempster Shafer Theory, Journal of Hydrology, 590, 125275,
587 <https://doi.org/10.1016/j.jhydrol.2020.125275>, 2020.
- 588 Guo, Y., Quan, L., Song, L., and Liang, H.: Construction of rapid early warning and comprehensive
589 analysis models for urban waterlogging based on AutoML and comparison of the other three machine
590 learning algorithms, J. Hydrol., 605, 127367, 2022a.
- 591 Guo, Y., Quan, L., Song, L., and Liang, H.: Construction of rapid early warning and comprehensive
592 analysis models for urban waterlogging based on AutoML and comparison of the other three machine
593 learning algorithms, J. Hydrol., 605, 127367, <https://doi.org/10.1016/j.jhydrol.2021.127367>, 2022b.
- 594 He, X., Zhao, K., and Chu, X.: AutoML: A survey of the state-of-the-art, Knowledge-Based Systems,
595 212, 106622, <https://doi.org/10.1016/j.knosys.2020.106622>, 2021.



- 596 Hsiao, S.-C., Chiang, W.-S., Jang, J.-H., Wu, H.-L., Lu, W.-S., Chen, W.-B., and Wu, Y.-T.: Flood risk
597 influenced by the compound effect of storm surge and rainfall under climate change for low-lying coastal
598 areas, *Science of the total environment*, 764, 144439, 2021.
- 599 Jordan, M. and Mitchell, T.: Machine learning: Trends, perspectives, and prospects, *Science*, 349, 255–
600 260, <https://doi.org/10.1126/science.aaa8415>, 2015.
- 601 Kanani-Sadat, Y., Arabsheibani, R., Karimipour, F., and Nasser, M.: A new approach to flood
602 susceptibility assessment in data-scarce and ungauged regions based on GIS-based hybrid multi criteria
603 decision-making method, *J. Hydrol.*, 572, 17–31, <https://doi.org/10.1016/j.jhydrol.2019.02.034>, 2019.
- 604 Kazienko, P., Lughofer, E., and Trawinski, B.: Editorial on the special issue “Hybrid and ensemble
605 techniques in soft computing: recent advances and emerging trends,” *Soft Comput.*, 19, 3353–3355,
606 <https://doi.org/10.1007/s00500-015-1916-x>, 2015.
- 607 Khadka, D., Babel, M. S., and Kamalamma, A. G.: Assessing the Impact of Climate and Land-Use
608 Changes on the Hydrologic Cycle Using the SWAT Model in the Mun River Basin in Northeast Thailand,
609 *Water*, 15, 3672, <https://doi.org/10.3390/w15203672>, 2023.
- 610 Khosravi, K., Shahabi, H., Pham, B. T., Adamowski, J., Shirzadi, A., Pradhan, B., Dou, J., Ly, H.-B.,
611 Gróf, G., Ho, H. L., Hong, H., Chapi, K., and Prakash, I.: A comparative assessment of flood
612 susceptibility modeling using Multi-Criteria Decision-Making Analysis and Machine Learning Methods,
613 *J. Hydrol.*, 573, 311–323, <https://doi.org/10.1016/j.jhydrol.2019.03.073>, 2019.
- 614 Lang, M., Barriendos, M., Llasat, M. C., Francés, F., Ouarda, T., Thorndycraft, V., Enzel, Y., Bardossy,
615 A., Coeur, D., and Bobée, B.: Use of Systematic, Palaeoflood and Historical Data for the Improvement
616 of Flood Risk Estimation. Review of Scientific Methods, *Nat. Hazards*, 31, 623–643,
617 <https://doi.org/10.1023/B:NHAZ.0000024895.48463.eb>, 2004.
- 618 Li, J., Cheng, K., Wang, S., Morstatter, F., Trevino, R. P., Tang, J., and Liu, H.: Feature Selection: A
619 Data Perspective, *ACM Comput. Surv.*, 50, 94:1-94:45, <https://doi.org/10.1145/3136625>, 2017.
- 620 Liu Jiafu and Zhang Bai: Progress of Rainstorm Flood Risk Assessment, *地理科学*, 35, 346–351,
621 <https://doi.org/10.13249/j.cnki.sgs.2015.03.013>, 2015.
- 622 Lu, H., Lu, X., Jiao, L., and Zhang, Y.: Evaluating urban agglomeration resilience to disaster in the
623 Yangtze Delta city group in China, *Sustainable Cities and Society*, 76, 103464, 2022.
- 624 Lundberg, S. M. and Lee, S.-I.: A Unified Approach to Interpreting Model Predictions, in: *Advances in*
625 *Neural Information Processing Systems*, 2017.



- 626 Mahmoud, S. H. and Gan, T. Y.: Urbanization and climate change implications in flood risk management:
627 Developing an efficient decision support system for flood susceptibility mapping, *Science of The Total*
628 *Environment*, 636, 152–167, <https://doi.org/10.1016/j.scitotenv.2018.04.282>, 2018.
- 629 Mei, C., Liu, J., Wang, H., Shao, W., Yang, Z., Huang, Z., Li, Z., and Li, M.: Flood risk related to
630 changing rainfall regimes in arterial traffic systems of the Yangtze River Delta, *Anthropocene*, 35,
631 100306, <https://doi.org/10.1016/j.ancene.2021.100306>, 2021.
- 632 Mia, Md. U., Rahman, M., Elbeltagi, A., Abdullah-Al-Mahbub, Md., Sharma, G., Islam, H. M. T., Pal,
633 S. C., Costache, R., Islam, A. R. Md. T., Islam, M. M., Chen, N., Alam, E., and Washakh, R. M. A.:
634 Sustainable flood risk assessment using deep learning-based algorithms with a blockchain technology,
635 *Geocarto International*, 38, 1–29, <https://doi.org/10.1080/10106049.2022.2112982>, 2023.
- 636 Milanesi, L., Pilotti, M., and Ranzi, R.: A conceptual model of people’s vulnerability to floods, *Water*
637 *Resources Res.*, 51, 182–197, <https://doi.org/10.1002/2014WR016172>, 2015.
- 638 Mirzaei, S., Vafakhah, M., Pradhan, B., and Alavi, S. J.: Flood susceptibility assessment using extreme
639 gradient boosting (EGB), Iran, *Earth Sci. Inf.*, 14, 51–67, <https://doi.org/10.1007/s12145-020-00530-0>,
640 2021.
- 641 Mishra, K. and Sinha, R.: Flood risk assessment in the Kosi megafan using multi-criteria decision
642 analysis: A hydro-geomorphic approach, *Geomorphology*, 350, 106861,
643 <https://doi.org/10.1016/j.geomorph.2019.106861>, 2020.
- 644 Morales-Torres, A., Escuder-Bueno, I., Andrés-Doménech, I., and Perales-Momparler, S.: Decision
645 Support Tool for energy-efficient, sustainable and integrated urban stormwater management,
646 *Environmental Modelling & Software*, 84, 518–528, <https://doi.org/10.1016/j.envsoft.2016.07.019>, 2016.
- 647 Munim, Z. H., Sørli, M. A., Kim, H., and Alon, I.: Predicting maritime accident risk using Automated
648 Machine Learning, *Reliab. Eng. Syst. Saf.*, 248, 110148, <https://doi.org/10.1016/j.ress.2024.110148>,
649 2024.
- 650 Nagarajah, T. and Poravi, G.: A Review on Automated Machine Learning (AutoML) Systems, in: 2019
651 IEEE 5th International Conference for Convergence in Technology (I2CT), 2019 IEEE 5th International
652 Conference for Convergence in Technology (I2CT), 1–6,
653 <https://doi.org/10.1109/I2CT45611.2019.9033810>, 2019.
- 654 Nayak, P. C., Sudheer, K. P., Rangan, D. M., and Ramasastri, K. S.: A neuro-fuzzy computing technique
655 for modeling hydrological time series, *J. Hydrol.*, 291, 52–66, 2004.



- 656 Özdemir, H., Baduna Koçyiğit, M., and Akay, D.: Flood susceptibility mapping with ensemble machine
657 learning: a case of Eastern Mediterranean basin, Türkiye, *Stoch. Env. Res. Risk A.*, 37, 4273–4290,
658 <https://doi.org/10.1007/s00477-023-02507-z>, 2023.
- 659 Raschka, S.: Model Evaluation, Model Selection, and Algorithm Selection in Machine Learning,
660 <https://doi.org/10.48550/arXiv.1811.12808>, 10 November 2020.
- 661 Rashidi Shikhteymour, S., Borji, M., Bagheri-Gavkosh, M., Azimi, E., and Collins, T. W.: A novel
662 approach for assessing flood risk with machine learning and multi-criteria decision-making methods,
663 *Appl. Geogr.*, 158, 103035, <https://doi.org/10.1016/j.apgeog.2023.103035>, 2023.
- 664 Sarro, F., Moussa, R., Petrozziello, A., and Harman, M.: Learning From Mistakes: Machine Learning
665 Enhanced Human Expert Effort Estimates, *IEEE Trans. Softw. Eng.*, 48, 1868–1882,
666 <https://doi.org/10.1109/TSE.2020.3040793>, 2022.
- 667 Scott, D., Hall, C. M., Rushton, B., and Gössling, S.: A review of the IPCC Sixth Assessment and
668 implications for tourism development and sectoral climate action, *J. Sustain. Tour.*, 0, 1–18,
669 <https://doi.org/10.1080/09669582.2023.2195597>, 2023.
- 670 Seemuangnam, A. and Lin, H.-L.: The impact of urbanization on urban flood risk of Nakhon
671 Ratchasima, Thailand, *Appl. Geogr.*, 162, 103152, <https://doi.org/10.1016/j.apgeog.2023.103152>, 2024.
- 672 Shafizadeh-Moghadam, H., Valavi, R., Shahabi, H., Chapi, K., and Shirzadi, A.: Novel forecasting
673 approaches using combination of machine learning and statistical models for flood susceptibility
674 mapping, *Journal of environmental management*, 217, 1–11, 2018.
- 675 Sinha, R., Bapalu, G. V., Singh, L. K., and Rath, B.: Flood risk analysis in the Kosi river basin, north
676 Bihar using multi-parametric approach of Analytical Hierarchy Process (AHP), *J. Indian Soc. Remote
677 Sens.*, 36, 335–349, <https://doi.org/10.1007/s12524-008-0034-y>, 2008.
- 678 Sun, B., Fang, C., Liao, X., Guo, X., and Liu, Z.: The relationship between urbanization and air pollution
679 affected by intercity factor mobility: A case of the Yangtze River Delta region, *Environ. Impact Assess.
680 Rev.*, 100, 107092, <https://doi.org/10.1016/j.eiar.2023.107092>, 2023.
- 681 Tang, Z., Wang, P., Li, Y., Sheng, Y., Wang, B., Popovych, N., and Hu, T.: Contributions of climate
682 change and urbanization to urban flood hazard changes in China's 293 major cities since 1980, *J. Environ.
683 Manage.*, 353, 120113, <https://doi.org/10.1016/j.jenvman.2024.120113>, 2024.



- 684 Vincent, A. M., K.s.s., P., and Jidesh, P.: Flood susceptibility mapping using AutoML and a deep learning
685 framework with evolutionary algorithms for hyperparameter optimization, *Appl. Soft Comput.*, 148,
686 110846, <https://doi.org/10.1016/j.asoc.2023.110846>, 2023.
- 687 Wagenaar, D., Curran, A., Balbi, M., Bhardwaj, A., Soden, R., Hartato, E., Mestav Sarica, G., Ruangpan,
688 L., Molinario, G., and Lallemand, D.: Invited perspectives: How machine learning will change flood risk
689 and impact assessment, *Nat. Hazard. Earth Sys.*, 20, 1149–1161, [https://doi.org/10.5194/nhess-20-1149-](https://doi.org/10.5194/nhess-20-1149-2020)
690 2020, 2020.
- 691 Wan, H., Zhong, Z., Yang, X., and Li, X.: Impact of city belt in Yangtze River Delta in China on a
692 precipitation process in summer: A case study, *Atmos. Res.*, 125–126, 63–75,
693 <https://doi.org/10.1016/j.atmosres.2013.02.004>, 2013.
- 694 Wang, M., Li, Y., Yuan, H., Zhou, S., Wang, Y., Adnan Ikram, R. M., and Li, J.: An XGBoost-SHAP
695 approach to quantifying morphological impact on urban flooding susceptibility, *Ecol. Indic.*, 156, 111137,
696 <https://doi.org/10.1016/j.ecolind.2023.111137>, 2023a.
- 697 Wang, M., Fu, X., Zhang, D., Chen, F., Liu, M., Zhou, S., Su, J., and Tan, S. K.: Assessing urban flooding
698 risk in response to climate change and urbanization based on shared socio-economic pathways, *Science
699 of The Total Environment*, 880, 163470, <https://doi.org/10.1016/j.scitotenv.2023.163470>, 2023b.
- 700 Wang, P., Li, Y., Yu, P., and Zhang, Y.: The analysis of urban flood risk propagation based on the
701 modified susceptible infected recovered model, *J. Hydrol.*, 603, 127121,
702 <https://doi.org/10.1016/j.jhydrol.2021.127121>, 2021.
- 703 Wang, T., Wang, H., Wang, Z., and Huang, J.: Dynamic risk assessment of urban flood disasters based
704 on functional area division—A case study in Shenzhen, China, *J. Environ. Manage.*, 345, 118787,
705 <https://doi.org/10.1016/j.jenvman.2023.118787>, 2023c.
- 706 Wang, Y., Liu, G., Guo, E., and Yun, X.: Quantitative Agricultural Flood Risk Assessment Using
707 Vulnerability Surface and Copula Functions, *Water*, 10, 1229, <https://doi.org/10.3390/w10091229>, 2018.
- 708 Xu, H., Hou, X., Pan, S., Bray, M., and Wang, C.: Socioeconomic impacts from coastal flooding in the
709 21st century China’s coastal zone: A coupling analysis between coastal flood risk and socioeconomic
710 development, *Sci. Total Environ.*, 917, 170187, 2024.
- 711 Yan, M., Yang, J., Ni, X., Liu, K., Wang, Y., and Xu, F.: Urban waterlogging susceptibility assessment
712 based on hybrid ensemble machine learning models: A case study in the metropolitan area in Beijing,
713 China, *J. Hydrol.*, 630, 130695, 2024.



714 Yang, W., Xu, K., Lian, J., Ma, C., and Bin, L.: Integrated flood vulnerability assessment approach based
715 on TOPSIS and Shannon entropy methods, *Ecol. Indic.*, 89, 269–280,
716 <https://doi.org/10.1016/j.ecolind.2018.02.015>, 2018.

717 Yang, X., Li, H., Zhang, J., Niu, S., and Miao, M.: Urban economic resilience within the Yangtze River
718 Delta urban agglomeration: Exploring spatially correlated network and spatial heterogeneity, *Sustainable*
719 *Cities and Society*, 103, 105270, <https://doi.org/10.1016/j.scs.2024.105270>, 2024.

720 Yuan, X., Chen, C., Lei, X., Yuan, Y., and Muhammad Adnan, R.: Monthly runoff forecasting based on
721 LSTM–ALO model, *Stoch. Env. Res. Risk A.*, 32, 2199–2212, [https://doi.org/10.1007/s00477-018-](https://doi.org/10.1007/s00477-018-1560-y)
722 [1560-y](https://doi.org/10.1007/s00477-018-1560-y), 2018.

723